Acousto-optical Scanning–Based High-Speed 3D Two-Photon Imaging *in Vivo*

Balázs Rózsa, MD, PhD, Gergely Szalay, and Gergely Katona

Institute of Experimental Medicine of the
Hungarian Academy of Sciences
Budapest, Hungary

SfN Society for Neuroscience

Rationale for Selecting Acousto-optical Scanning for *in Vivo* Network Measurement in Three Dimensions

Several novel technologies have been developed for the three-dimensional (3D) readout of fast populations and dendritic activities. These include liquid lenses (Grewe et al., 2011), holographic scanning (Nikolenko et al., 2008), Roller Coaster Scanning (Katona et al., 2011), piezo scanning with sinusoidal resonance (Gobel et al., 2007), deformable mirrors, temporal and spatial multiplexing (Cheng et al., 2011), axicon or planar illumination–based imaging (Holekamp et al., 2008), fast *z*-scanning based on an axially moving mirror (Botcherby et al., 2012), simultaneous multiview light-sheet microscopy (Tomer et al., 2012), and optical fiber acousto-optical deflector (AOD)–based 3D scanning (Rózsa et al., 2007). However, only acousto-optical scanning can increase the product of the measurement speed and the signal collection efficiency by several orders of magnitude, as compared with classical raster scanning.

More quantitatively, random-access scanning increases measurement speed and signal collection efficiency in the following way:

$$\frac{(\textit{measurement speed})*(\textit{signal collection}) \cong (\textit{total image volume})}{(\textit{volume covered by the scanning points})}$$

where "signal collection" is defined as the amount of the detected fluorescent photons in a given time interval from a given spatial location, and the "volume covered by the scanning points" is the convolution of the point spread function (PSF) and the preselected scanning points. In a typical *in vivo* measurement, when we consider using a 450 × 450 × 650 μm^3 scanning volume with a 0.47–1.9 µm and 2.49–7.9 µm axial resolution (Katona et al., 2012), and simultaneously measure approximately 100 locations, random access scanning will provide a 2,106,000–46,534-fold, on average an increase of six orders of magnitude, in the product of measurement speed and signal collection efficiency. According to the current state of the technology (which now provides an ~1 mm^3 scanning volume with high-numerical-aperture [NA] objectives), this increase could be even larger: more than 1,000,000,000 per locations. No other available 3D method with high spatial resolution and deep penetration capability can provide a similar increase in the product of the measurement speed and the signal collection efficiency.

A further advantage of 3D acousto-optical microscope technology is that it is based on single-spot two-photon activation, which allows whole-field detection with high-quantum-efficiency photomultiplier tube (PMTs). Therefore, photons scattered from deep layers of the tissue can also be collected with high sensitivity, which is essential to realize imaging through the whole cortex. Moreover, the position of the PSF can be finely adjusted, with 50–100 nm precision (Katona et al., 2012), to any spatial coordinates during acousto-optical scanning. Therefore, there is no limitation in *z*-planes and coordinates, which enables a highly precise measurement of neuronal activity by eliminating neuropil contamination.

Principles

The phrase "acousto-optic" refers to the field of optics that studies the interaction between sound and light waves. In imaging, it means especially the diffraction of a laser beam through ultrasonic grating. The acousto-optical effect is produced by the periodic change in the refractive index of the medium (usually tellurium dioxide), which results from the sound-wave-induced pressure fluctuation in the crystal. This grating diffracts the light beam just like normal optical grating.

Acousto-optical deflection

AODs spatially control the optical beam using ultrasonic waves. During operation, the acoustic frequency is varied in a way that results in an acoustic-frequency-dependent diffraction of the laser beam. The change of the diffraction angle is given by the following formula:

$$\Delta\Theta_d = \frac{\lambda}{v}\Delta f$$

where λ is the optical wavelength of the beam, ν is the velocity of the acoustic wave, and Δf is the change of the sound frequency (Fig. 1).

In practice, AODs or acousto-optical modulators (AOMs) are used. AOMs modulate only the amplitude of the sound waves, whereas AODs are able to adjust both the amplitude and the frequency.

Acousto-optical focusing

Besides deflection, AODs can be used for fast focal-plane shifting (Kaplan et al., 2001; Vucinic and Sejnowski, 2007; Katona et al., 2012; Cotton et al., 2013; Fernandez-Alfonso et al., 2014). If the optical aperture is filled with acoustic waves whose frequency increases as a function of time (chirped wave), different portions of the optical beam are deflected

NOTES

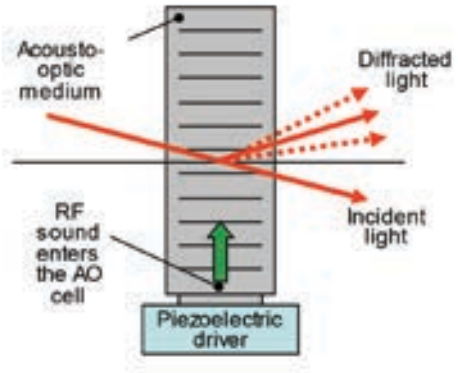

Figure 1. Operating principle of acousto-optical (AO) deflectors. RF, radiofrequency.

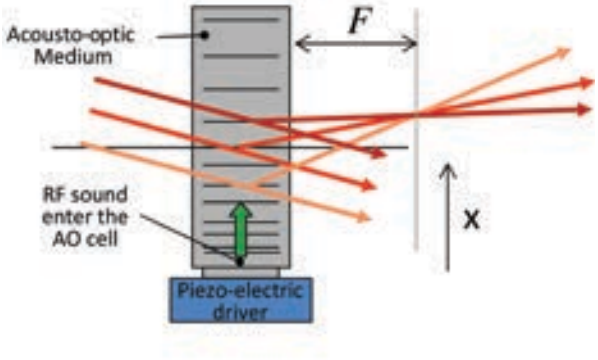

Figure 2. Acousto-optical (AO) focusing. RF, radiofrequency.

in different directions (Fig. 2); thus, a focusing or defocusing effect occurs, depending on the frequency slope (sweep rate) of the chirped acoustic wave.

The focal length of acousto-optical lens can be calculated from the sweep rate. The focal distance (F) of the deflectors can be defined as follows:

$$F = \frac{v^2 T_{scan}}{2\lambda\Delta f}$$

where λ is the optical wavelength of the beam, ν is the velocity of the acoustic wave, Δf is the change of the sound frequency, and T_{scan} is the modulation rate of the sound frequency (Kaplan et al., 2001).

To keep the focus stable, the frequency gradient should be preserved in the crystal. The frequency should therefore be continuously increased (or decreased) at the piezoelectric driver to preserve the focal distance. This will result in a lateral drift of the focal spot that can be easily compensated by a second AOD with a counterpropagating acousto-optical wave. The optical grid generated within the AOD is equivalent to a cylindrical lens. In 3D two-photon microscopy, it is necessary to scan points. Therefore, a combination of two perpendicularly oriented cylindrical lenses with the same focal distance is required. And, because both acousto-optical lenses (x, y) require drift compensation, 3D microscopes need at least four AO deflectors ($x1$, $y1$, $x2$, $y2$). The four AO deflectors can be optically coupled using "afocal projections" (telescopes with two lenses where the distance between the lenses is equal to the sum of each lens's focal length) and air in different combinations. The largest scanning volume can be reached by grouping the deflectors into two functionally distinct groups (z-focusing and lateral scanning), which are coupled by one afocal projection (Katona et al., 2012).

Controlling 3D acousto-optical scanning

To focus the excitation beam to a given x,y,z-coordinate, the four AODs should be driven synchronously with varying frequency voltage signals. Because AODs have limited electrical bandwidths, the changing frequency can be maintained only for a limited time before the frequency has to be abruptly reset. This sudden change of frequency results in an improperly formed focal spot, and thus can be considered "dead time" (Fig. 3). The length of this period is defined by the time the acoustic wave travels through the aperture of the crystal, usually ~5–30 µs.

The position and the movement of the focal point are determined by eight values. Four of them control the starting acoustic frequency on the four AOD drivers, while the other four define the frequency ramp speeds (chirping). All eight parameters are updated in every sweep cycle (typically 33.6 µs is used; the minimum is 5–10 µs). The starting frequencies and the chirps together define the xyz position of the focal spot and its xy movement speed (drifting). During every sweep cycle, all PMT channels are sampled multiple times. The ratio of the dead time (offset time) to the measurement time (when the focal spot has already been formed and is ready for imaging) depends on the z-level and is optimal at the nominal focal plane of the objective.

In the simplest case, the goal is to attain a steady focal spot without lateral drifting (in random-access scanning mode). In this scanning mode, PMT data are averaged, and one value is created for each measurement cycle, corresponding to a single point in xyz. Thus, this mode enables random-access 3D point scanning, which is ideal for monitoring neuronal network activity. More complex measurement modes are possible when one lets the focal spot drift, such as during Multiple 3D Trajectory Scanning.

The 3D Acousto-optical Microscope

Realization of the optical pathway

In order to realize the optical pathway of a 3D microscope, one must create a 3D random-access laser scanning two-photon microscope that simultaneously satisfies two different needs in the largest possible scanning volume. The first need is to record activity across the dendritic tree of a single neuron at high spatial and temporal resolution in 3D in a central core (~290 × 290 × 200 μm^3) of the scanning volume and to do so in such a way that dendritic spines remain resolvable. The second need is to record activity in a more extensive volume (now >1100 × 1100 × 3000 μm^3 in transparent samples) at high speed but at a lower resolution, in order to capture the activities of a large number of cell bodies in a neuronal population.

Following the arrangement suggested by the model, a large-aperture (15–17 mm) optical assembly was constructed (Figs. 4, 5). Here, a Ti:S laser with automated dispersion compensation provides the laser pulses. A Faraday isolator blocks the coherent backreflections. A four-prism sequence (Proctor and Wise, 1992) adds a large negative second- and third-order dispersion (−72,000 fs^2 and −40,000 fs^3, respectively) in order to precompensate for pulse broadening caused by the optical elements of the system (dispersion compensation unit; Fig. 5).

An automated beam stabilization unit (see Laser Beam Stabilization, below) is necessary to precisely stabilize the laser beam of the long optical pathway and to cancel out subtle thermal drift errors. The beam stabilization unit is built from position sensors (quadrant detectors) and motorized mirrors, wired in a feedback loop. The beam is then magnified by a beam expander to match the large apertures (15 mm) of the first pair of AODs. These AODs form two orthogonal electric cylinder lenses filled with continuously changing frequency ("chirped") acoustic waves (Kaplan et al., 2001), which are used for *z*-focusing (AO *z*-focusing unit).

Next, laser beams from the *x* and *y* cylindrical lenses are projected onto the *x* and *y* AO deflectors (17 mm apertures) of the 2D scanning unit, respectively, by telecentric projection. This 2D-AO scanning unit performs lateral scanning and compensates for the lateral drift of the focal spot generated by the cylindrical lenses during *z*-focusing, i.e., drift compensation (Kaplan et al., 2001). The angular

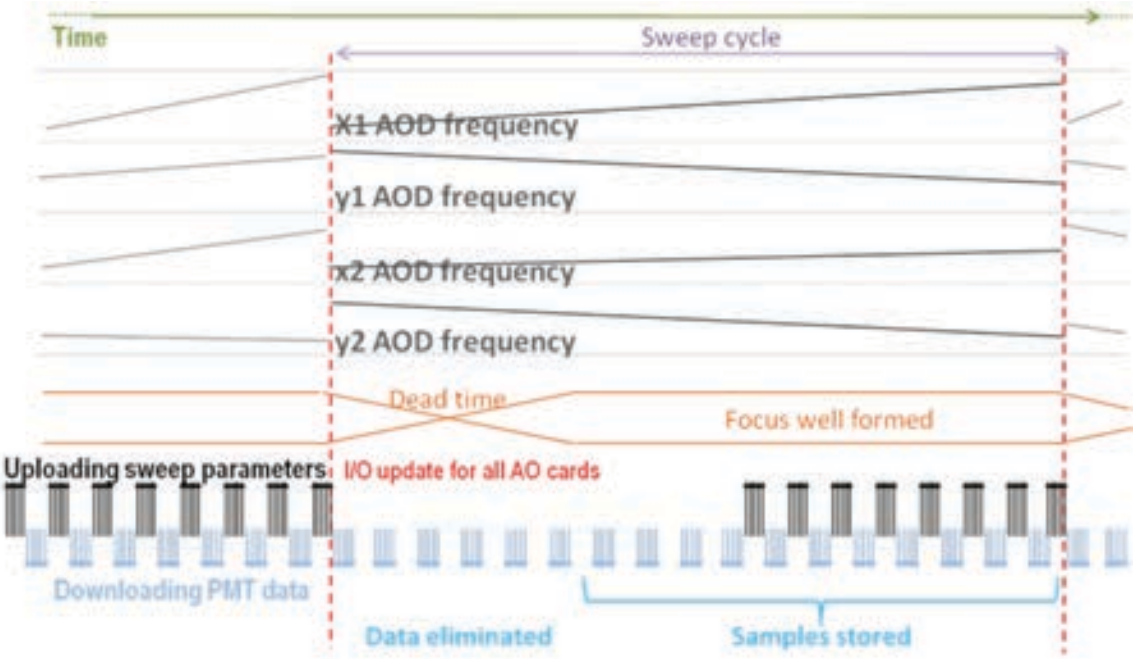

Figure 3. Driving functions and timing of operation of the four-deflector sequence. Top, The four upper traces show the frequency modulation of the sine wave as a function of time for the four AO deflectors (*x*1, *y*1, *x*2, *y*2) within 1.5 sweep cycles. This results in "dead" times and periods when focus is well formed (orange). Bottom, PMT data are continuously collected and transferred to the computer; however, PMT data collected during the dead time period are eliminated during the acquisition. Red dashed lines, synchronous frequency reset of all driver functions.

NOTES

dispersion compensation unit optically links the 2D-AO scanning unit with the objective. Modeling helped us design and manufacture a custom lens made of high-dispersion glass with aspheric and conic surfaces which, combined with a telecentric projection of the AO scanner unit to the objective's back aperture, diminishes the angular dispersion introduced by the AO devices at off-axis positions ($x,y \neq 0$). Then, the 3D scanning system is coupled to a 2D two-photon microscope in which fluorescent signals are collected by PMTs fixed directly onto the objective arm for high photon-collection efficiency (Fig. 5). In contrast to previous AO microscope designs, we have also taken advantage of the active optical elements to dynamically compensate for optical errors (e.g., astigmatism, field curvature, angular dispersion, chromatic aberration) that increased spatial resolution especially during AO *z*-focusing (at $z \neq 0$ planes by a factor of ~2–3; Fig. 4).

We determined the optimal compensation parameters in advance for each point of the scanning volume and loaded them into the driver electronics accordingly. During this optimization process, we varied the parameters of the chirped sine driver function at each of the four deflectors in order to maximize the fluorescence intensity and the sharpness of the fluorescent beads used during this calibration. Spatial resolution in the whole scanning volume was also increased by the large optical apertures used throughout the system, and ~20% of this increase resulted solely from the use of large AOD apertures (Fig. 4). In contrast to the dominantly *z*-focusing-dependent effect of dynamic error compensation, the angular dispersion compensation unit decreased the PSF in off-axis positions when compared with a simple two-lens telecentric projection (Fig. 4*b*). These factors that decrease the PSF inherently increase the lateral field of view (Fig. 4*a*).

One difference between the system described here and previous designs is that the AODs form functionally and physically different groups. Z-focusing is carried out by the first AO pair, whereas lateral scanning is performed entirely by the second pair (2D-AO scanning unit). This arrangement increased the diameter of the lateral scanning range by a factor of ~2.7 (Fig. 4*a*). Furthermore, not only electronic driver function but also deflector geometry, TeO_2 crystal orientation, and bandwidth differed between deflectors of the *z*-focusing and the 2D-AO scanning unit. Altogether, these factors increased the diameter of the lateral scanning range by ≤720 μm using the Olympus 20× objective and >1100 μm using the Nikon 16× objective.

Materials and methods

Figure 5 is a schematic block diagram of the microscope, which was realized according to detailed optical modeling (Katona et al., 2012). Laser pulses

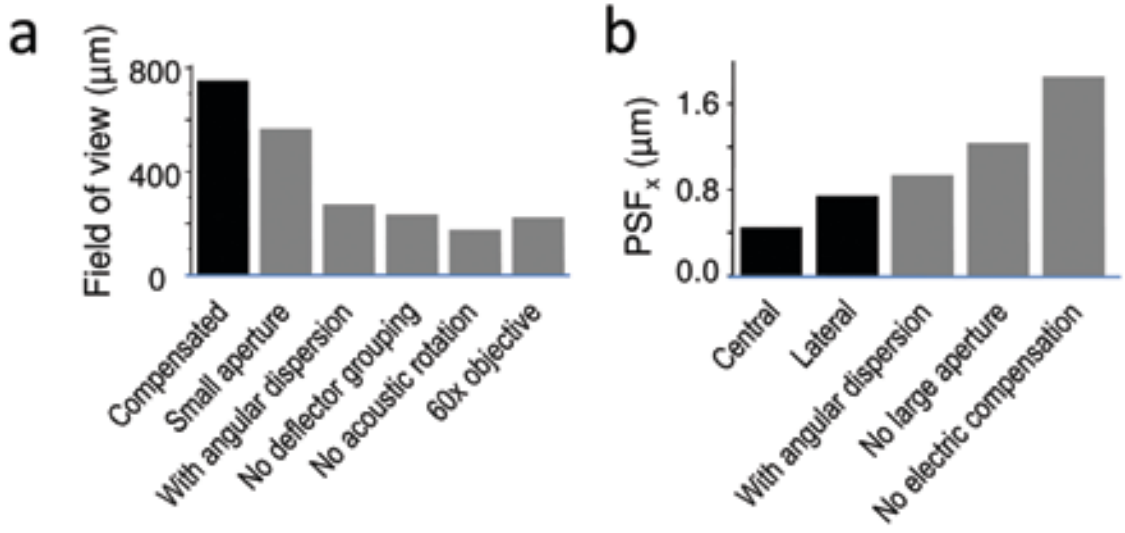

Figure 4. Characterization of the two-photon AO microscope setup. ***a,*** The maximal field of view ("compensated") is shown when both deflector pairs were used for deflection ("no deflector grouping") or when optically rotated deflectors ("no acoustic rotation"), small aperture objectives (60×), no angular dispersion compensation ("with angular dispersion") or small aperture AODs were used ("small aperture"). ***b,*** The compensated PSF size along the *x*-axis (PSF_x) ("central") at (*x, y, z*) = (150, 150, 100) μm coordinates ("lateral") or when no angular dispersion compensation ("with angular dispersion"), no electronic compensation ("no electric compensation"), or reduced AO apertures ("no large apertures") were applied. Reprinted with permission from Katona et al. (2012), their Fig. 1*b, c*.

are provided by a Mai Tai DeepSee femtosecond laser (Spectra-Physics, Santa Clara, CA). The optimal wavelength range is 740–880 nm (but can also be extended ≤1064 nm). Pulse backreflection to the laser source is eliminated by a Faraday isolator (BB8-5I, Electro-Optics Technology, Traverse City, MI). Next, the beam position is stabilized using two motorized mirrors (m, Fig. 5) (Agilis Series, AG-M100N, Newport), which stabilize the position of the light transmitted by two backside custom-polished broadband mirrors (BB2-E03, Thorlabs, Newton, NJ) on the surface of two quadrant detectors (q, Fig. 5) (PDQ80A, Thorlabs). The positioning feedback loop (U12, LabJack Corporation, Lakewood, CO) is controlled by a program written in LabVIEW (National Instruments). The beam is expanded by two achromatic lenses arranged in a Galilean telescope (f = −75 mm, ACN254-075-B, Thorlabs; f = 200 mm, NT47319, Edmund Optics; distance = 125.62 mm) to match the large apertures of the first pair of AODs (15 mm). Mirrors, λ/2 wave plates and holders, are purchased from Thorlabs and Newport. AODs have been custom designed and manufactured at the Budapest University of Technology and Economics. Achromatic telecentric relay lenses were purchased from Edmund Optics (f_{TC} = 150 mm, NT32-886). Achromatic scan and tube lenses were chosen from Edmund Optics (f = 250 mm, NT45-180) and Olympus (f = 210 mm), respectively. The AO-based 3D scanner system is attached to the top of a

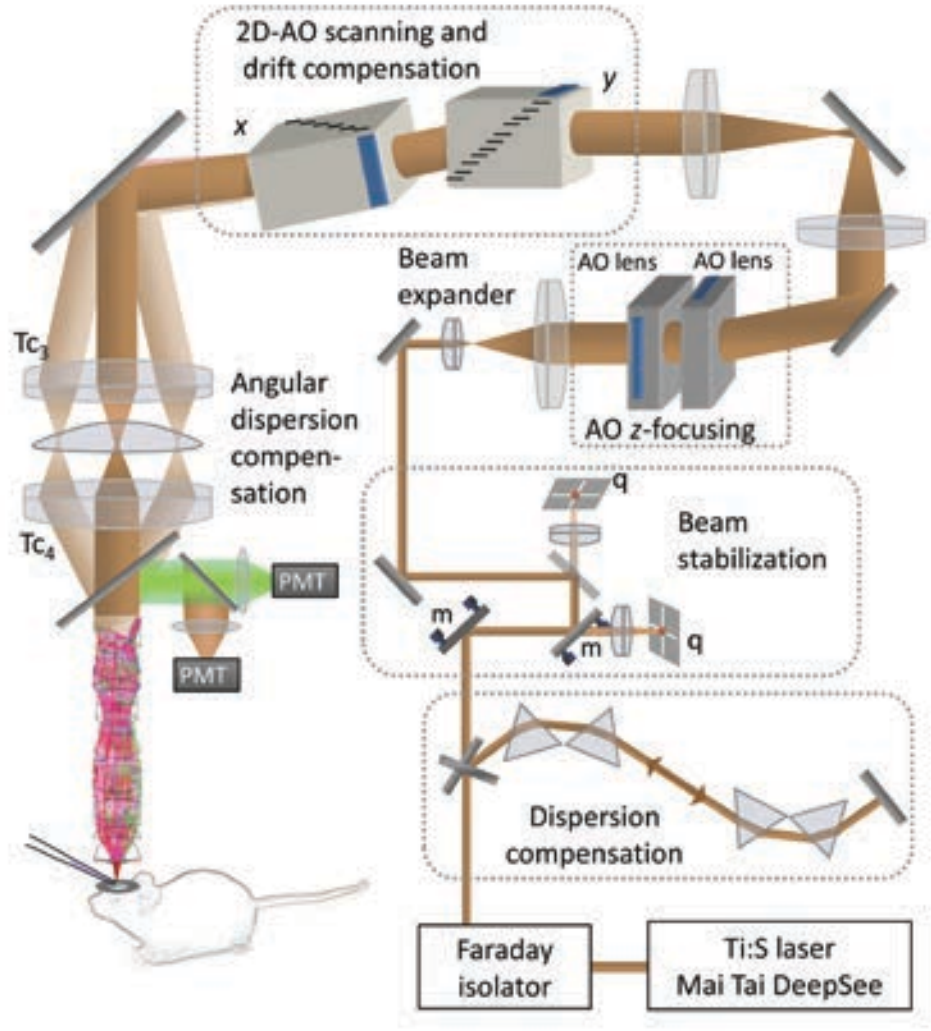

Figure 5. Design and characterization of the two-photon AO microscope setup. Material-dispersion compensation is adjusted using a four-prism compressor and a Ti:S laser. A Faraday isolator eliminates coherent backreflections, while a Ti:S laser with automated dispersion compensation provides the laser pulses. Motorized mirrors (m) stabilize the position of the beam light on the surface of two quadrant detectors (q) before the beam expander. Two AODs optimized for diffraction efficiency control the z-focusing of the beam (AO z-focusing). A 2D-AO scanner unit performs x–y scanning and drift compensation during z-scanning. A spherical field lens in the second telecentric lens system ($Tc_{3,4}$) provides additional angular dispersion compensation. Reprinted with permission from Katona et al. (2012), their Fig. 1*a*.

NOTES

galvanometer-based, upright two-photon microscope (Femto2D Alba, Femtonics, Budapest) using custom-designed rails. AO sweeps are generated by direct digital synthesizer chips (AD9910, 1 GSPS, 14-bit, Analog Devices, Norwood, MA) integrated into the modular electronics system of the microscope using FPGA elements (Xilinx).

Red and green fluorescence are separated by a dichroic filter (39 mm, 700dcxru, Chroma Technology, Bellows Falls, VT) and are collected by GaAsP PMTs custom-modified to efficiently collect scattered photons (PMT, H7422P-40-MOD, Hamamatsu Photonics, Hamamatsu City, Japan), fixed directly onto the objective arm (traveling detector system). In *in vitro* experiments, the forward-emitted fluorescence can also be collected by 2 inch aperture detectors positioned below the condenser lens (Femto2D Alba, Femtonics). Signals of the same wavelength measured at the epifluorescent and transfluorescent positions are added. The large aperture objectives, XLUMPlanFI20×/0.95 (Olympus, 20×, NA = 0.95) and CFI75 LWD 16×W (Nikon, 16×, NA = 0.8), provide the largest scanning volume (Katona et al., 2012). The maximal output laser power in front of the objective is ~400 mW (at 875 nm).

Laser beam stabilization

The role of the laser beam stabilization loop is to compensate for the thermal drift and small vibration of the laser resonator and optical elements. The system comprises several elements that are highly sensitive to the incidence angle. To compensate for the translation and angle deviation of the beam, a pair of two-axis piezo mirrors with two quadrant detectors act as a reference.

Prism compressor

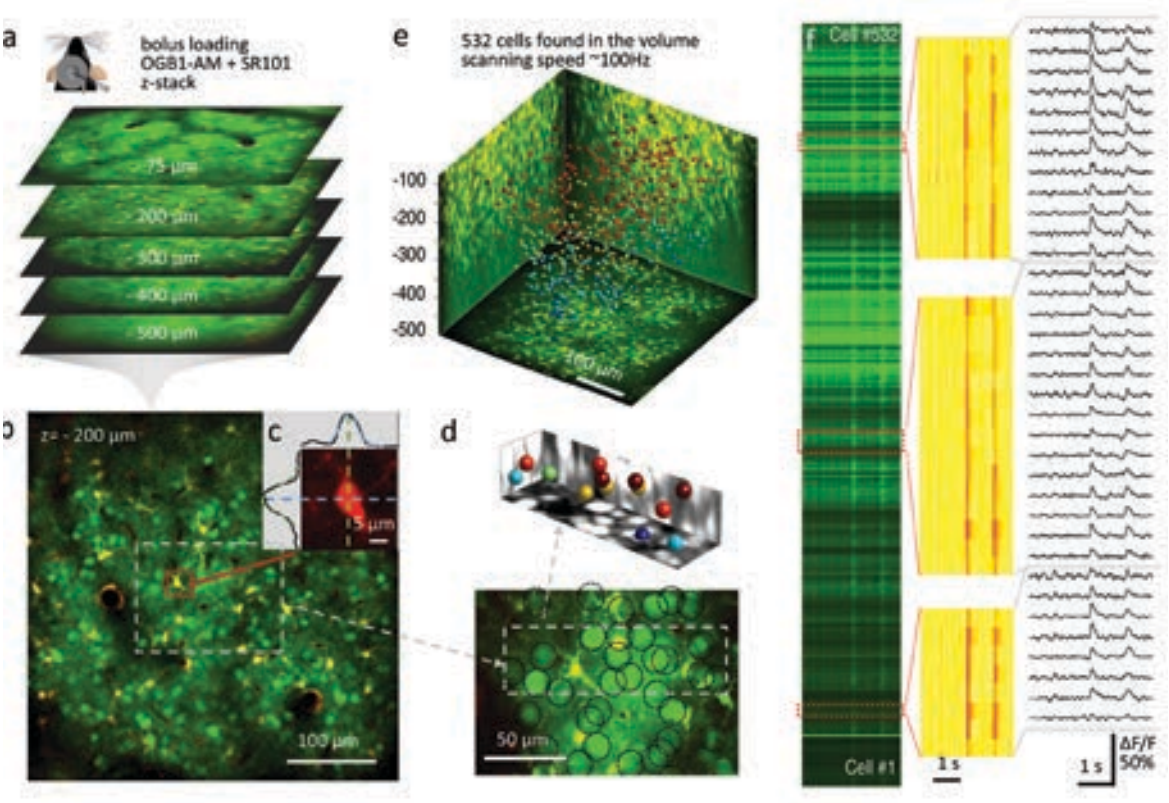

Figure 6. High-speed 3D calcium imaging of spontaneous neuronal network activity *in vivo*. ***a,*** Top, Sketch of *in vivo* experimental arrangement. Bottom, Staining by bolus loading (Oregon Green BAPTA [OGB]-1-AM and SR-101) in mouse primary visual cortex (V1). Five representative planes at different depths are imaged with 3D-AO scanning. Depths are measured relative to the pia. ***b,*** Example of an image plane at 200 µm depth showing neurons (green) and glial cells (magenta and white). Scale bar, 100 µm. ***c,*** Image and intensity profiles of a preselected bright glial cell used to establish the measurement coordinate system. Scale bar, 5 µm. ***d,*** Bottom, 35 µm *z*-projection of the region marked in ***b.*** Scale bar, 50 µm. Top, Neuronal somata detected with the aid of an algorithm in a subvolume (shown with projections, neurons in white and glial cells in black). ***e,*** Maximal intensity side- and *z*-projections of the entire *z*-stack (400 × 400 × 500 µm^3) with autodetected cell locations (spheres) color-coded in relation to depth. The set detection threshold yields 532 neurons. Scale bar, 100 µm. ***f,*** Spontaneous neuronal network activity measured in the 532 cells in ***e.*** Left, example of a raw trace in which each line corresponds to a cell. Spatially normalized traces (middle) and corresponding Ca^{2+} transients (right). Calibration, 1 s. Reprinted with permission from Katona et al. (2012), their Fig. 4.

The material dispersion compensation problem is solved by a motorized prism compressor. The four-prism unit (Fig. 5) adds a large negative dispersion to precompensate the pulse broadening caused by the optical elements of the system. Total compensation depends on the given wavelength. Approximately 72,000 fs^2 second-order group delay dispersion (GDD) and ~40,000 fs^3 third-order dispersion (TOD) compensation is required; the precise amount depends on the objective used and the central wavelength. We also added a two-pass, four-prism compressor (Proctor and Wise, 1992; Rózsa et al., 2007) that provides a fixed compensation amount at a given wavelength. A mechanically fixed compressor unit could be combined with the variable compensation provided by the DeepSee unit of the Mai Tai laser (Spectra-Physics) to confer dynamically adjustable dispersion compensation for an optimum fluorescence signal. Alternatively, motorizing the four-prism sequences would enable the omission of the DeepSee unit and thereby provide ~10% higher infrared transmission.

Experiments

AO scanning technology can be beneficial in biological experiments in which one would like to perform functional imaging in 3D from sparse regions of interest (ROIs) relatively far from each other. For example, it is beneficial when one would like to follow the activity of multiple dendritic segments of a single neuron (Chiovini et al., 2014), to measure activity from large neuronal networks (Katona et al., 2012; Cotton et al., 2013; Fernandez-Alfonso et al., 2014), or to perform simultaneous measurements of somas and dendritic spines (Katona et al., 2012; Fernandez-Alfonso et al., 2014).

Acousto-optical scanning methods

Multiple scanning modes have been developed for AO scanning that can also be used in different combinations as needed by the experimental protocol.

Random-access point scanning

Random-access point scanning is one of the most convenient applications for imaging neuronal networks in 3D. In the first step, a reference *z*-stack image is acquired (Fig. 6*a*). In the second step, points can be preselected for fast 3D measurements (Figs. 6*b*–*e*). Once a region with well-stained cells is identified, one can select one or more reference structures (typically, a brightly red-fluorescing glial cell), scan it in 3D, and define the 3D origin [(0, 0, 0) coordinate] of the recording as the center of this glial cell (Fig. 6). In order to compensate for tissue drift, one needs to rescan the "origin-glia" cell regularly during an experiment and move it back into the original position (0,0,0) by moving the microscope table and the objective. 3D Ca^{2+} responses recorded

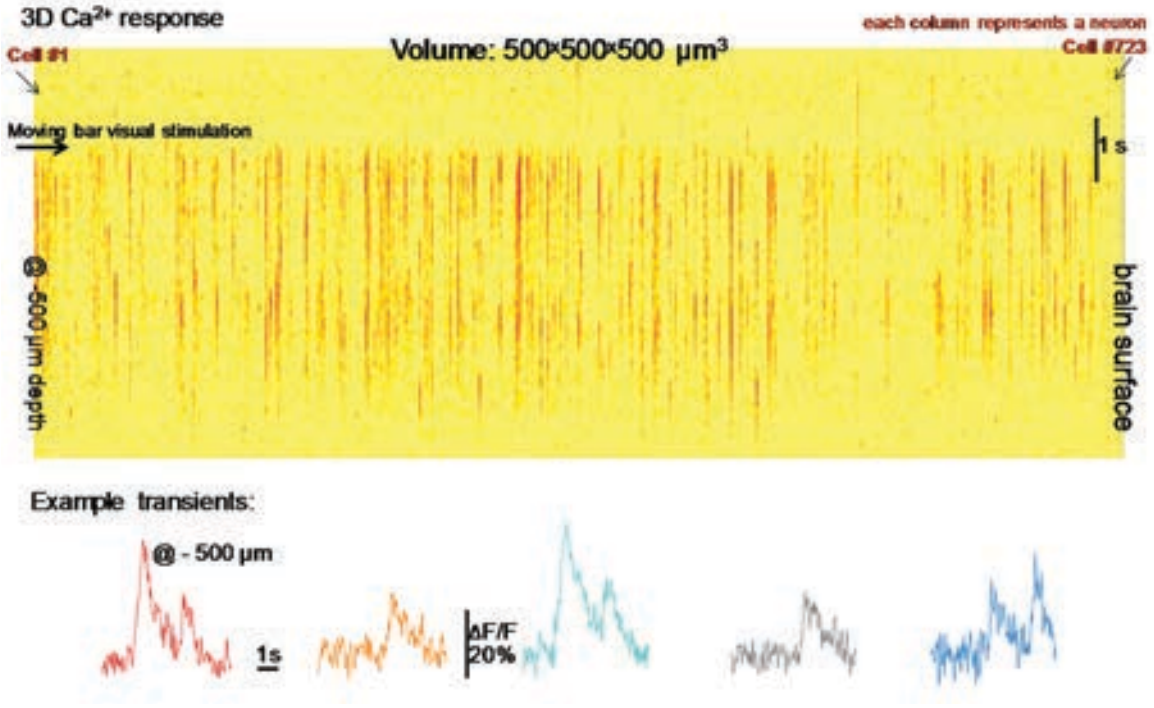

Figure 7. High-speed 3D random-access *in vivo* recording of 723 neurons that were simultaneously recorded. The exemplified transients demonstrated that the signal-to-noise ratio is preserved even at the bottom of the scanning volume (at –500 µm depth from the surface in this example). Calibration, 1 s.

NOTES

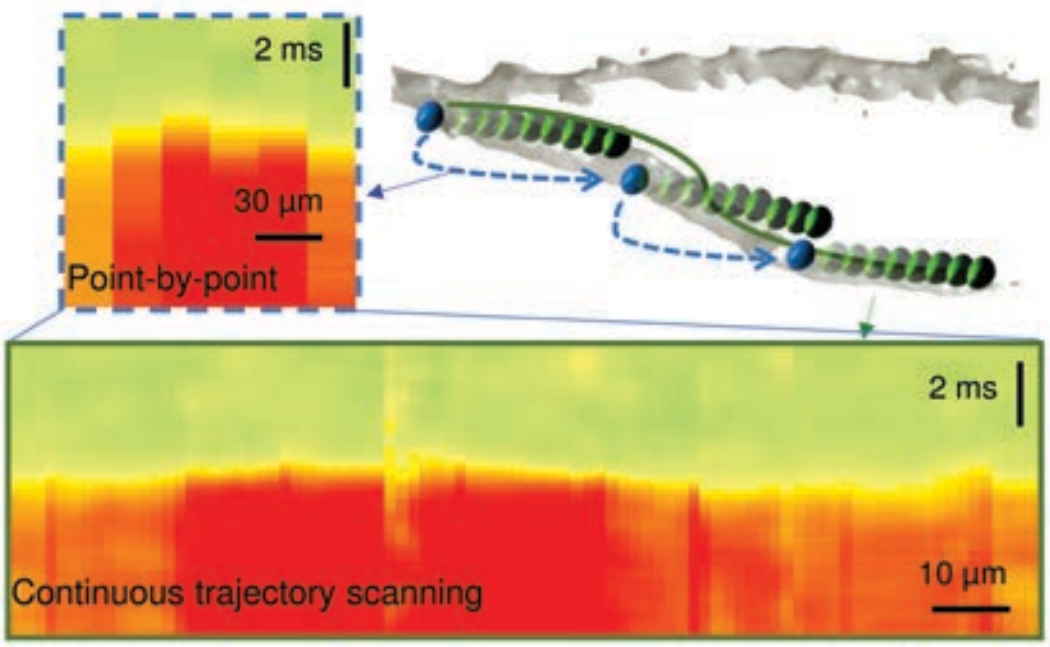

Figure 8. Point-by-point and continuous 3D trajectory scanning of dendritic segments. Top right, Schema of the scanning modes (blue point-by-point scanning; green, continuous scanning). Top left, Example of Ca^{2+} responses measured by point-by-point. Scale bar, 30 µm. Bottom, continuous trajectory modes. Traces were spatially normalized. Scale bar, 10 µm; calibration, 2 ms. Reprinted with permission from Katona et al. (2012), their Fig. 3*f*.

simultaneously in multiple points can be plotted as curves (Fig. 6*f*, right panel), or alternatively, responses following spatial normalization can be shown as images (Fig. 6*f*, middle panel; Fig. 7).

Frame scanning in 3D

One of the basic measurement modes that can be realized with a 3D-AO microscope is frame scanning. In this mode, one can freely move or rotate arbitrary areas in 3D using the real (by moving the objective) and virtual (by focusing with the AODs at a fixed objective position) z for focusing. Because frame-scanning mode is relatively slow in 3D, this mode can be used to find and preselect ROIs for the subsequent fast 3D measurements. Multiple areas situated in multiple layers can be selected and measured simultaneously.

Multiple 3D trajectory scanning

Multiple 3D trajectory scanning mode was developed for simultaneously measuring multiple neuronal processes. There are two realizations of 3D trajectory scanning. In the continuous trajectory scanning mode, instead of jumping between preselected points (as during point scanning), one lets the focal spot drift along neuronal processes (Fig. 8). In this way, information is collected with a much higher spatial discretization within the same time interval.

XYZ *or volume imaging*

It is possible to capture volumetric data by successively capturing xy images at different z positions. The jump between the z-planes can be obtained by using either the real or the virtual focus. The first will result in better optical quality; therefore, it can be used at the end of experiments if only volume information is acquired. However, if one would like to perform fast 3D line scanning, 3D frame scanning, or random-access scanning, the z-stack should be obtained with virtual focusing in order to precisely preserve the coordinates of the cells for the fast 3D-AO scanning because the coordinate system of 3D-AO microscopes is distorted. Alternatively, a coordinate transformation is needed to match the two types of z-stacks to each other.

Movement correction

During long *in vivo* measurements, sample drifting can cause problems. Because in the random-access scanning paradigm one usually measures from a single point per cell or dendritic segment, the imaging quality can be very sensitive to sample movements. Quick timescale movements can be reduced only by preparation techniques. However, slow timescale drifts can be compensated for using software tools. For this compensation, reference objects are needed, which can consists of bright, well-defined objects in

the sample (Fig. 6c). These can be either a bright nonspecific object or a bright cell from which one does not expect activity-dependent fluorescence change. During compensation, one keeps the *xyz* center of this object in a given point inside the volume. Using this compensation method, a slow drift of the sample can be compensated for because, in this case, all points move together along the *xyz* coordinates; however, torsion of the sample cannot be compensated. In practice, this means that from one set of points, it is possible to take measurements for a couple of hours without significant drop in the image quality. This compensation can be performed manually or with software tools.

Automatic cell finding

In the simplest cases, cells can be categorized according to their dye content as measured by fluorescence, which is possible on multiple channels. In the most straightforward case, OGB1-AM and SR-101 dyes are bolus-loaded into the animal. In this technique, neuronal cells can be detected from their elevated green fluorescence and decreased red fluorescence. We normalize green and red fluorescent channel data from each image in the stack and then scale and shift them so that its 10th and 90th percentiles match 0 and 1. Background correction is done by oversmoothing an image and subtracting it from the original. Next, we subtract the red-channel data from the green and filter each layer of the stack again. The resulting stack is then searched for local maxima with an adaptive threshold. If two selected locations are closer than a given distance threshold, only one is kept.

In the algorithmically most complex cases, cell coordinates should be found according to their response to a (visual) stimulus (e.g., when using currently available channelrhodopsin [ChR] variants). In such cases, as a first step, random-access volume scanning is done on locations evenly spread over the field of view, sampling the space at approximately every 10 µm so that one point is sampled from each cell. Visual stimulation is then presented to the animal to drive the normally silent cells and reveal their location. In a second step, a finer mesh is scanned around the active locations to more precisely outline the cell locations and their center.

Simultaneous cell-attached recording

The decay time of currently available calcium indicators is usually not fast enough in *in vivo* conditions to resolve bursts of action potentials (APs); single AP resolution is also problematic in most instances. However, the amplitudes of the Ca^{2+} peaks are proportional to the number of the APs. To measure this relationship, one needs to detect APs preferentially using juxtacellular recording, which is a relatively noninvasive method. Such measurements show that although the amplitude of the Ca^{2+} signal is linearly proportional to the number of APs, the proportion coefficient for the different dyes (and even for different loading levels) can be quite variable (Fig. 9). Similar variability can be detected in GCaMP6 animals.

3D acousto-optical imaging of dendrites

The second main field of application for AO microscopes is dendritic imaging. This method can be used to measure propagation speeds; to simultaneously

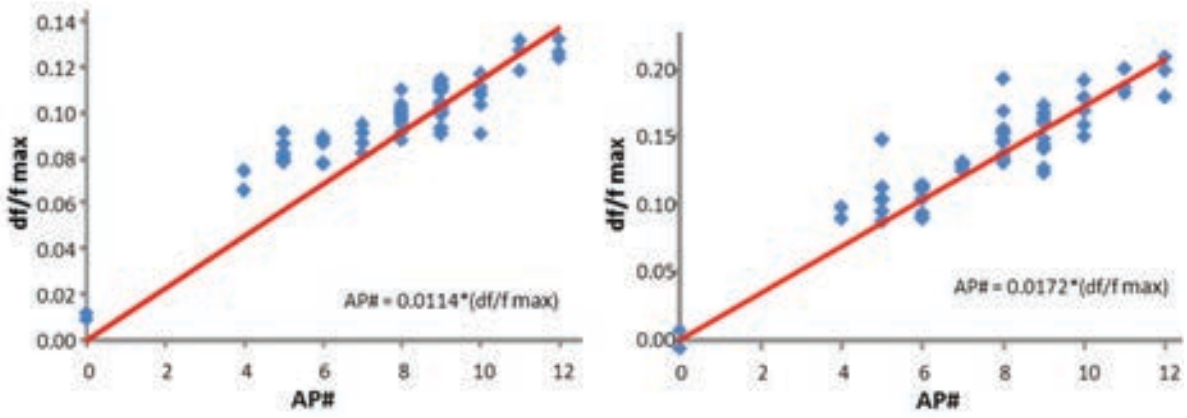

Figure 9. Maximum df/f_{max}-dependent AP number for two different cells in two different types of OGB bolus loading. Note the difference in the slope of the responses.

NOTES

follow large-scale spontaneous dendritic events, such as sharp-wave-associated dendritic spikes in multiple dendritic segments (Chiovini et al., 2014); to study dendritic plasticity; or to measure dendritic spines *in vivo*. 3D fluorescence measurements and two-photon uncaging experiments in thin dendritic segments and spines are very sensitive to spatial misalignments because even displacements below the resolution limit can induce significant changes in responses. It is possible to compensate for these errors using high-resolution motion artifact compensation. Once a region for dendritic measurements has been identified, one can select two or more reference lines with high angular deviation that cross both the imaged and the neighboring bright dendritic structures. Fluorescence data are collected preferentially in the red channel. To compensate for tissue drift, one needs to repeatedly measure the spatial distribution of fluorescence along these reference lines; one should also minimize the discrepancy relative to the original distributions using cross-correlation, using either an automatic or a manual process. Alternatively, a set of reference points depicting fluorescent local maxima in the sample need to be selected at the beginning of the measurement and their x,y,z-coordinates continuously optimized during measurements in order to obtain the maximum average fluorescence level.

Measuring propagation speed along dendrites

Random-access AO scanning enables the measurement of, for example, fast-propagating calcium waves both along the dendrites (by measuring a few points relatively far from each other) and along the dendrites with fast temporal resolution. Cells need to be loaded with a high-concentration, low-affinity calcium sensor (Fluo-5F, 400 μM) in whole-cell patch–clamp arrangement to perform measurements with good signal-to-noise ratio with fast onset times of the calcium events. In this example, we selected points along the dendritic tree of one pyramidal neuron in 3D (Fig. 9). We held the cell in current–clamp mode and evoked APs by somatic current injection. At the same time, we near-simultaneously measured dendritic Ca^{2+} signals associated with the backpropagating action potential (BAP) by repetitively scanning the selected 3D coordinates at several tens of kHz. We calculated the velocity of the BAP from the latency of the Ca^{2+} transients and the distance from the soma. Average BAP propagation speed differed at 23°C and 33°C (164 ± 13 μm ms^{-1} [n = 9] versus 227 ± 14 μm ms^{-1} [n = 13]; p = 0.006, t-test, Fig. 10).

Looking to the Future

Although the "hardware" for the AO microscope is nearing a theoretical maximum that can be realized with a given objective lens, there is a strong untapped potential in AO scanning still to be worked out:

- Developing novel software algorithms that could realize complex measurement modes;
- Applying the technology to larger FOV objectives;
- Developing novel correction methods for eliminating movement artifacts;
- Implementing adaptive optics;
- Improving lasers and fluorescent dyes to gain access to the entire thickness of the cortex;
- Simplifying the system to lower its costs and maintenance requirements;
- Improving wavelength tunability; and
- Providing simultaneous imaging and photostimulation in multiple regions.

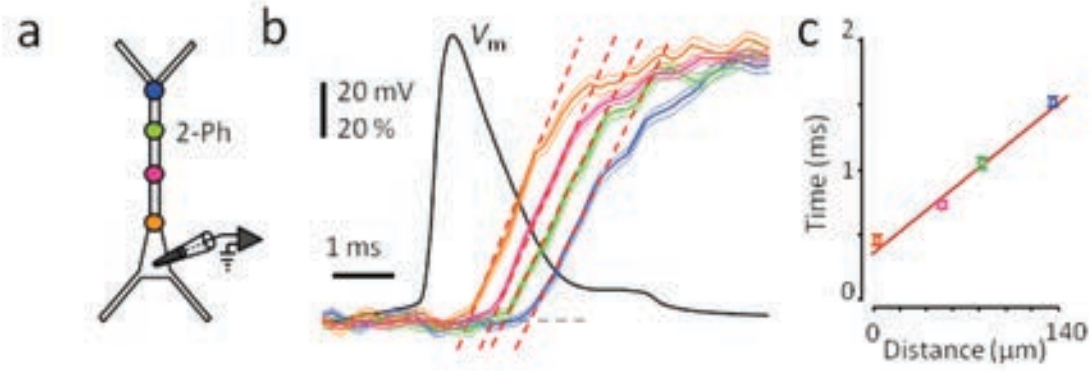

Figure 10. Measurement of propagation speed of BAP in apical dendrites. ***a,*** Experimental arrangement for signal propagation experiments. Signal propagation speed was measured by somatic whole-cell current-clamp (V_m, black) and 3D two-photon calcium imaging (orange, pink, green, and blue). ***b,*** AP peak triggered average of normalized dendritic Ca^{2+} transients induced by bAPs (mean ± SEM; n = 54; top). Linear fits (red dashed lines) define onset latency times. ***c,*** Onset latency times (mean ± SEM; n = 54) of Ca^{2+} transients in ***b*** as a function of dendritic distance. Linear fit = average propagation speed. Reprinted with permission from Katona et al. (2012), their Figs. 2*c, d, g.*

In addition to these improvements, 3D recordings will need to be performed in symbiosis with neuronal network and dendritic modeling; 3D recorded data must be explained by neuronal network and dendritic modeling; and, conversely, measurements must be performed according modeling predictions (Almog and Korngreen, 2014; Chiovini et al., 2014).

Acknowledgment

Parts of this chapter were published in Katona et al. (2012), Fast two-photon *in vivo* imaging with three-dimensional random-access scanning in large tissue volumes. Nat Methods 9:201–208.

References

Almog M, Korngreen A (2014) A quantitative description of dendritic conductances and its application to dendritic excitation in layer 5 pyramidal neurons. J Neurosci 34:182–196.

Botcherby EJ, Smith CW, Kohl MM, Debarre D, Booth MJ, Juskaitis R, Paulsen O, Wilson T (2012) Aberration-free three-dimensional multiphoton imaging of neuronal activity at kHz rates. Proc Natl Acad Sci U S A 109:2919–2924.

Cheng A, Goncalves JT, Golshani P, Arisaka K, Portera-Cailliau C (2011) Simultaneous two-photon calcium imaging at different depths with spatiotemporal multiplexing. Nat Methods 8:139–142.

Chiovini B, Turi GF, Katona G, Kaszas A, Palfi D, Maak P, Szalay G, Szabo MF, Szabo G, Szadai Z, Kali S, Rózsa B (2014) Dendritic spikes induce ripples in parvalbumin interneurons during hippocampal sharp waves. Neuron 82:908–924.

Cotton RJ, Froudarakis E, Storer P, Saggau P, Tolias AS (2013) Three-dimensional mapping of microcircuit correlation structure. Front Neural Circuits 7:151.

Fernandez-Alfonso T, Nadella KM, Iacaruso MF, Pichler B, Ros H, Kirkby PA, Silver RA (2014) Monitoring synaptic and neuronal activity in 3D with synthetic and genetic indicators using a compact acousto-optic lens two-photon microscope. J Neurosci Methods 222:69–81.

Gobel W, Kampa BM, Helmchen F (2007) Imaging cellular network dynamics in three dimensions using fast 3D laser scanning. Nat Methods 4:73–79.

Grewe BF, Voigt FF, van 't Hoff M, Helmchen F (2011) Fast two-layer two-photon imaging of neuronal cell populations using an electrically tunable lens. Biomedical optics express 2:2035–2046.

Holekamp TF, Turaga D, Holy TE (2008) Fast three-dimensional fluorescence imaging of activity in neural populations by objective-coupled planar illumination microscopy. Neuron 57:661–672.

Kaplan A, Friedman N, Davidson N (2001) Acousto-optic lens with very fast focus scanning. Opt Lett 26:1078–1080.

Katona G, Kaszas A, Turi GF, Hajos N, Tamas G, Vizi ES, Rózsa B (2011) Roller Coaster Scanning reveals spontaneous triggering of dendritic spikes in CA1 interneurons. Proc Natl Acad Sci U S A 108:2148–2153.

Katona G, Szalay G, Maak P, Kaszas A, Veress M, Hillier D, Chiovini B, Vizi ES, Roska B, Rózsa B (2012) Fast two-photon *in vivo* imaging with three-dimensional random-access scanning in large tissue volumes. Nat Methods 9:201–208.

Nikolenko V, Watson BO, Araya R, Woodruff A, Peterka DS, Yuste R (2008) SLM Microscopy: Scanless Two-Photon Imaging and Photostimulation with Spatial Light Modulators. Front Neural Circuits 2:5.

Proctor B, Wise F (1992) Quartz prism sequence for reduction of cubic phase in a mode-locked Ti:Al(2)O(3) laser. Opt Lett 17:1295–1297.

Rózsa B, Katona G, Vizi ES, Varallyay Z, Saghy A, Valenta L, Maak P, Fekete J, Banyasz A, Szipocs R (2007) Random access three-dimensional two-photon microscopy. Appl Opt 46:1860–1865.

Tomer R, Khairy K, Amat F, Keller PJ (2012) Quantitative high-speed imaging of entire developing embryos with simultaneous multiview light-sheet microscopy. Nat Methods 9:755–763.

Vucinic D, Sejnowski TJ (2007) A compact multiphoton 3D imaging system for recording fast neuronal activity. PLoS One 2:e699.